# Theoretical analysis of acoustic stop bands in two-dimensional periodic scattering arrays

You-Yu Chen and Zhen Ye
*Wave Phenomena Laboratory, Department of Physics, National Central University, Chungli, Taiwan 32054*
(Received 17 April 2001; published 29 August 2001)

This paper presents a theoretical analysis of the recently reported observation of acoustic stop bands in two-dimensional scattering arrays [Robertson and Rudy, J. Acoust. Soc. Am. **104**, 694 (1998)]. A self-consistent wave scattering theory, incorporating all orders of multiple scattering, is used to obtain the wave transmission. The band structures for the regular arrays of cylinders are computed using the plane-wave expansion method. The theoretical results compare favorably with the experimental data.

DOI: 10.1103/PhysRevE.64.036616 PACS number(s): 43.20.+g

## I. INTRODUCTION

When propagating through media containing many scatterers, waves will be scattered by each scatterer. The scattered waves will be scattered again by other scatterers. This process is repeated to establish an infinite iterative pattern of rescattering between scatterers, forming a multiple scattering process [1]. Multiple scattering of waves is responsible for a wide range of fascinating phenomena, including such as twinkling light in the evening sky and modulation of ocean ambient sound [2,3]. On smaller scales, phenomena such as electron transport in impure solids [4] are also results of multiple scattering. When waves propagate through media with periodic structures, the multiple scattering leads to the phenomenon of band structures. That is, waves can propagate in certain frequency ranges and follow certain dispersion relations, while in other frequency regimes wave propagation may be stopped. The former ranges are called allowed bands and the latter the forbidden bands.

The wave dispersion bands were first studied for electronic waves in solids, providing the basis for understanding the properties of conductors, semiconductors, and insulators [5]. In late 1980s, it became known that such a wave band phenomenon is also possible for classical waves. The studies on manipulation of classical waves were started with electromagnetic waves in media with periodically modulated refractive indices [6]. Since then, optical wave bands have been extensively studied, yielding a rich body of literature [7]. The theoretical calculations have proven to match well with the experimental observations [8]. The modulation of optical waves by periodic media has led to a number of practical applications including the design of photonic crystals [9], the optical fibers [10], and waveguide devices [11]. Recently, it has also been found that a living organism may also display a remarkable photonic engineering [12].

In contrast, research on acoustic wave band structures has just started (for example, refer to [13]). Although theoretical computations of band structures have been well documented for periodic acoustic structures [14], the experimental work was only recent, and to date only a limited number of measurements have been reported. One of the first observations was made on acoustic attenuation by a minimalist sculpture [15] and further studied in the laboratory [16]. The authors obtained a sound attenuation spectrum, which was later verified by the band structure computation [17,18]. Recently, acoustic band structures have been further measured for acoustic transmission through two-dimensional (2D) periodic arrays of metal cylinders placed in the air [13]. The authors reported experimental observation of acoustic stop bands and wave transmission for both square and triangular arrays. The impulse response technique was used to determine the transmission over a broad frequency band width, whereas the acoustic dispersion relation was extracted from the phase information.

The main purpose of this paper is to provide a theoretical investigation of sound transmission by 2D arrays of rigid cylinders in air in line with the experiment described by Robertson and Rudy [13], providing a direct comparison of the acoustic transmission between theory and experiment. For the purpose, we employ a self-consistent multiple scattering theory [19] to compute the acoustic transmission through arrays of scattering cylinders. Meanwhile, the acoustic band structures are computed using the plane-wave method well prescribed by Kushwaha [14]. We will show that the theoretical results agree very well with the observation.

## II. FORMULATION OF THE PROBLEM

### A. Acoustic scattering by arrays of parallel cylinders

Consider $N$ straight identical cylinders located at $\vec{r}_i$ with $i=1,2,\ldots,N$ to form either a regular lattice (or a random array) perpendicular to the $x$-$y$ plane; the regular arrangement can be adjusted to comply with the experiment [13]. There are two types of the regular arrangements of the cylinders: the square lattice and the triangular lattice. The cylinders are along the $z$ axis. An acoustic source transmitting monochromatic waves is placed at $\vec{r}_s$, some distance from the array. The scattered wave from each cylinder is a response to the total incident wave composed of the direct wave from the source and the multiply scattered waves from other cylinders. The final wave reaches a receiver located at $\vec{r}_r$ is the sum of the direct wave from the source and the scattered waves from all the cylinders. The cylinders used in the experiment are metal cylinders. Numerical computation verifies that for acoustic scattering, the effect due to the shear modulus is negligible for such a cylinder in air. This has also been confirmed by experiments [16]. When the shear waves

 

are ignored, the exact solution for the scattering process can be conveniently formulated, following Twersky [19].

To exactly reproduce the experimental data, it would be necessary to know the information about the apparatus, the acoustic pulses generated, the lab environment, and the arrangement of the sounding and receiving devices. As the information is not readily available and is also unnecessary for the present theoretical investigation, we make certain reasonable simplifications.

For simplicity yet without compromising generality, we approximate the acoustic source as a line source located at origin, i.e., $\vec{r}_s=0$, the numerical computation indicates that the difference between a line source and a plane wave is not essential. Without the cylinders, the wave is governed by

$$(\vec{\nabla}^2+k^2)G(\vec{r})=-4\pi\delta^{(2)}(\vec{r}), \tag{1}$$

In the cylindrical coordinates, the solution is

$$G(\vec{r})=i\pi H_0^{(1)}(kr). \tag{2}$$

where $H_0^{(1)}$ is the zeroth order Hankel function of the first kind. In this section, $i$ stands for $\sqrt{-1}$.

With $N$ cylinders located at $\vec{r}_i$ $(i=1,2,\ldots,N)$, the scattered wave from the $j$th cylinder can be written as

$$p_s(\vec{r},\vec{r}_j)=\sum_{n=-\infty}^{\infty} i\pi A_n^j H_n^{(1)}(k|\vec{r}-\vec{r}_j|)e^{in\phi_{\vec{r}-\vec{r}_j}}, \tag{3}$$

where $H_n^{(1)}$ is the $n$th order Hankel function of the first kind, $A_n^i$ is the coefficient to be determined, and $\phi_{\vec{r}-\vec{r}_j}$ is the azimuthal angle of the vector $\vec{r}-\vec{r}_i$ relative to the positive $x$ axis.

The total wave incident around the $i$th scatterer $p_{in}^i(\vec{r})$ is a superposition of the direct contribution from the source $p_0(\vec{r})=G(\vec{r})$ and the scattered waves from all other scatterers

$$p_{in}^i(\vec{r})=p_0(\vec{r})+\sum_{j=1,j\neq i}^{N} p_s(\vec{r},\vec{r}_j). \tag{4}$$

In order to seperate the governing equations into modes, we can express the total incident wave in term of the modes about $\vec{r}_i$:

$$p_{in}^i(\vec{r})=\sum_{n=-\infty}^{\infty} B_n^i J_n(k|\vec{r}-\vec{r}_i|)e^{in\phi_{\vec{r}-\vec{r}_i}}. \tag{5}$$

The expansion is in terms of Bessel functions of the first kind $J_n$ to ensure that $p_{in}^i(\vec{r})$ does not diverge as $\vec{r}\to\vec{r}_i$. The coefficients $B_n^i$ are related to the $A_n^j$ in Eq. (3) through Eq. (4). A particular $B_n^i$ represents the strength of the $n$th mode of the total incident wave on the $i$th scatterer with respect to the $i$th scatterer's coordinate system (i.e., around $\vec{r}_i$). In order to isolate this mode on the right-hand side of Eq. (4), and thus determine a particular $B_n^i$ in terms of the set of $A_n^j$, we need to express $p_s(\vec{r},\vec{r}_j)$, for each $j\neq i$, in terms of the modes with respect to the $i$th scatterer. In other words, we want $p_s(\vec{r},\vec{r}_j)$ in the form

$$p_s(\vec{r},\vec{r}_j)=\sum_{n=-\infty}^{\infty} C_n^{j,i} J_n(k|\vec{r}-\vec{r}_i|)e^{i\phi_{\vec{r}-\vec{r}_i}}. \tag{6}$$

This can be acheived (i.e., $C_n^{j,i}$ expressed in terms of $A_n^i$) through the following addition theorem [20]

$$H_n^{(1)}(k|\vec{r}-\vec{r}_j|)e^{in\phi_{\vec{r}-\vec{r}_j}}=e^{in\phi_{\vec{r}_i-\vec{r}_j}}\sum_{l=-\infty}^{\infty} H_{n-l}^{(1)}(k|\vec{r}_i-\vec{r}_j|)\times e^{-il\phi_{\vec{r}_i-\vec{r}_j}}J_l(k|\vec{r}-\vec{r}_i|)e^{il\phi_{\vec{r}-\vec{r}_i}}. \tag{7}$$

Taking Eq. (7) into Eq. (3), we have

$$p_s(\vec{r},\vec{r}_j)=\sum_{n=-\infty}^{\infty} i\pi A_n^j e^{in\phi_{\vec{r}_i-\vec{r}_j}}\sum_{l=-\infty}^{\infty} H_{n-l}^{(1)}(k|\vec{r}_i-\vec{r}_j|)\times e^{-il\phi_{\vec{r}_i-\vec{r}_j}}J_l(k|\vec{r}-\vec{r}_i|)e^{il\phi_{\vec{r}-\vec{r}_i}}. \tag{8}$$

Or by switching the order of summation, we have

$$p_s(\vec{r},\vec{r}_j)=\sum_{l=-\infty}^{\infty}\left[\sum_{n=-\infty}^{\infty} i\pi A_n^j H_{n-l}^{(1)}(k|\vec{r}_i-\vec{r}_j|)e^{i(n-l)\phi_{\vec{r}_i-\vec{r}_j}}\right]\times J_l(k|\vec{r}-\vec{r}_i|)e^{il\phi_{\vec{r}-\vec{r}_i}}. \tag{9}$$

Comparing with Eq. (6), we see that

$$C_n^{j,i}=\sum_{l=-\infty}^{\infty} i\pi A_l^j H_{l-n}^{(1)}(k|\vec{r}_i-\vec{r}_j|)e^{i(l-n)\phi_{\vec{r}_i-\vec{r}_j}}. \tag{10}$$

Now we can relate $B_n^i$ to $C_n^{j,i}$ (and thus to $A_l^j$) through Eq. (4). First note that through the addition theorem the source wave can be written,

$$\begin{aligned} p_0(\vec{r}) &= i\pi H_0^{(1)}(kr) \\ &= i\pi\sum_{l=-\infty}^{\infty} H_{-l}^{(1)}(k|\vec{r}_i|)e^{-il\phi_{\vec{r}_i}}J_l(k|\vec{r}-\vec{r}_i|)e^{il\phi_{\vec{r}-\vec{r}_i}} \\ &= \sum_{l=-\infty}^{\infty} S_l^i J_l(k|\vec{r}-\vec{r}_i|)e^{il\phi_{\vec{r}-\vec{r}_i}}, \end{aligned} \tag{11}$$

where

$$S_l^i=i\pi H_{-l}^{(1)}(k|\vec{r}_i|)e^{-il\phi_{\vec{r}_i}}. \tag{12}$$

Matching coefficients in Eq. (4) and using Eqs. (5), (6), and (11), we have

$$B_n^i=S_n^i+\sum_{j=1,j\neq i}^{N} C_n^{j,i}, \tag{13}$$

or, expanding $C_n^{j,i}$,

$$B_n^i = S_n^i + \sum_{j=1,j\neq i}^{N} \sum_{l=-\infty}^{\infty} i\pi A_l^j H_{l-n}^{(1)}(k|\vec{r}_i - \vec{r}_j|) e^{i(l-n)\phi_{\vec{r}_i-\vec{r}_j}}. \tag{14}$$

At this stage, both the $S_n^i$ are known, but both $B_n^i$ and $A_l^j$ are unknown. Boundary conditions will give another equation relating them.

The boundary conditions are that the pressure and the normal velocity be continuous across the interface between a scatterer and the surrounding medium. The total wave outside the $i$th scatterer is $p_{ext} = p_{in}^i(\vec{r}) + p_s(\vec{r},\vec{r}_i)$. The wave inside the $i$th scatterer can be expressed as

$$p_{int}^i(\vec{r}) = \sum_{n=-\infty}^{\infty} D_n^i J_n(k_1^i|\vec{r} - \vec{r}_i|) e^{in\phi_{\vec{r}-\vec{r}_i}}. \tag{15}$$

The boundary conditions are then

$$p_{ext}|_{\partial\Omega^i} = p_{int}|_{\partial\Omega^i} \tag{16}$$

and

$$\frac{1}{\rho}\frac{\partial p_{ext}}{\partial n}\bigg|_{\partial\Omega^i} = \frac{1}{\rho_1^i}\frac{\partial p_{int}}{\partial n}\bigg|_{\partial\Omega^i}, \tag{17}$$

where $\partial\Omega^i$ is the boundary of the $i$th scatterer, $k$ and $\rho$ are the wave number and density of the surrounding medium, and $k_1^i$ and $\rho_1^i$ are the wave number and density of the $i$th scatterer, respectively. Using Eqs. (3), (5), and (15), multiplying both sides of the boundary condition equations by $e^{in\phi_{\vec{r}-\vec{r}_i}}$, and integrating over the boundary $\partial\Omega^i$, we have for the case of circular cylindrical scatterers,

$$B_n^i J_n(ka^i) + i\pi A_n^i H_n^{(1)}(ka^i) = D_n^i J_n(ka^i/h^i), \tag{18}$$

$$B_n^i J_n'(ka^i) + i\pi A_n^i H_n^{(1)'}(ka^i) = \frac{1}{g^i h^i} D_n^i J_n'(ka^i/h^i). \tag{19}$$

Here $a^i$ is the radius of the $i$th cylinder, $g^i = \rho_1^i/\rho$ is the density ratio, and $h^i = k/k_1^i = c_1^i/c$ is the sound speed ratio for the $i$th cylinder. Elimination of $D_n^i$ gives

$$B_n^i = i\pi\Gamma_n^i A_n^i, \tag{20}$$

where

$$\Gamma_n^i = \left[\frac{H_n^{(1)}(ka^i)J_n'(ka^i/h^i) - g^i h^i H_n^{(1)'}(ka^i) J_n(ka^i/h^i)}{g^i h^i J_n'(ka^i) J_n(ka^i/h^i) - J_n(ka^i) J_n'(ka^i/h^i)}\right]. \tag{21}$$

If we define

$$T_n^i = S_n^i/i\pi = H_{-n}^{(1)}(k|\vec{r}_i|) e^{-in\phi_{\vec{r}_i}} \tag{22}$$

and

$$G_{l,n}^{i,j} = H_{l-n}^{(1)}(k|\vec{r}_i - \vec{r}_j|) e^{i(l-n)\phi_{\vec{r}_i-\vec{r}_j}}, \quad i \neq j, \tag{23}$$

then Eq. (14) becomes

$$\Gamma_n^i A_n^i - \sum_{j=1,j\neq i}^{N} \sum_{l=-\infty}^{\infty} G_{l,n}^{i,j} A_l^j = T_n^i. \tag{24}$$

If the value of $n$ is limited to some finite range, then this is a matrix equation for the coefficients $A_n^i$. Once solved, the total wave at any point outside all cylinders is

$$p(\vec{r}) = i\pi H_0^{(1)}(k|\vec{r}|) + \sum_{i=1}^{N} \sum_{n=-\infty}^{\infty} i\pi A_n^i H_n^{(1)}(k|\vec{r} - \vec{r}_i|) e^{in\phi_{\vec{r}-\vec{r}_i}}. \tag{25}$$

We must stress that total wave expressed by Eq. (25) incorporate all orders of multiple scattering. We note, however, that an inclusion of the lowest order in multiple scattering may be sufficient for certain situations (J. Sánchez-Dehesa, private communication). We also emphasize that the above derivation is valid for any configuration of the cylinders. In other words, Eq. (25) works for situations that the cylinders can be placed either randomly or orderly.

### B. Band structures of regular arrays of cylinders

For a regular array of the cylinders, band structures for the wave propagation appear. The band structures can be readily computed by the plane-wave method [14]. Though the method has been well documented by Kushwaha [14], for the sake of convenience we outline the approach as follows.

The wave equation is

$$\vec{\nabla}\cdot\left[\frac{1}{\rho(\vec{r})}\vec{\nabla}p(\vec{r})\right] + \frac{\omega^2}{\rho(\vec{r})c^2(\vec{r})}p(\vec{r}) = 0, \tag{26}$$

where $\rho(\vec{r})$ and $c(\vec{r})$ are the mass density and sound speed, respectively; both are modulated by the periodic structures, i.e., inside the cylinders the values are that of the cylinders, while outside the cylinders they take the values of the medium. According to Bloch's theorem [5], the solution of the pressure field has the Bloch form

$$p(\vec{r}) = e^{i\vec{K}\cdot\vec{r}} \sum_{\vec{G}} \phi_{\vec{K}}(\vec{G}) e^{i\vec{G}\cdot\vec{r}}, \tag{27}$$

where $\vec{K}$ is termed as the Bloch wave vector, $\vec{G}$ is the reciprocal lattice vector [5]. The summation is made for all possible reciprocal vectors.

For the periodic structures, both $\rho^{-1}$ and $(\rho c^2)^{-1}$ in Eq. (26) can be expanded by discrete plane waves as follows:

$$\frac{1}{\rho(\vec{r})} = \sum_{\vec{G}} \sigma(\vec{G}) e^{i\vec{G}\cdot\vec{r}}, \quad \text{and} \quad \frac{1}{\rho(\vec{r})c^2(\vec{r})} = \sum_{\vec{G}} \eta(\vec{G}) e^{i\vec{G}\cdot\vec{r}}. \tag{28}$$

As $\rho(\vec{r})$ and $c(\vec{r})$ are known parameters, both $\sigma(\vec{G})$ and $\eta(\vec{G})$ can be determined from an inverse Fourier transform.

Substituting Eqs. (27) and (28) into Eq. (26), we obtain

$$\sum_{\vec{G}'} [\sigma(\vec{G}-\vec{G}')(\vec{K}+\vec{G})\cdot(\vec{K}+\vec{G}')-\eta(\vec{G}-\vec{G}')\omega^2]\phi_{\vec{K}}(\vec{G}') = 0, \tag{29}$$

which has the matrix form

$$\sum_{\vec{G}'} \Gamma_{\vec{G},\vec{G}'}\phi_{\vec{K}}(\vec{G}') = 0.$$

The dispersion relation connecting the frequency $\omega$ and the wave vector $\vec{K}$ is determined by the secular equation

$$\begin{aligned}\det[\Gamma_{\vec{G},\vec{G}'}] &= \det[\sigma(\vec{G}-\vec{G}')(\vec{K}+\vec{G})\cdot(\vec{K}+\vec{G}') \\ &\quad -\eta(\vec{G}-\vec{G}')\omega^2]_{\vec{G},\vec{G}'} \\ &= 0,\end{aligned} \tag{30}$$

where ''det'' denotes the determinant. Equation (30) leads to the dispersion relation between the frequency $\omega(\vec{K})$ and the wave vector $\vec{K}$. We use the standard eigenvalue inversion method in the IMSL library to solve Eq. (30) to obtain the dispersion relation.

### III. NUMERICAL RESULTS

Numerical computation has been performed to obtain the transmitted acoustic wave and the acoustic band structures. In particular, the numerical computation has been carried out for the experimental situations [13].

First we consider the transmitted waves described by Eq. (25). In the simulation, all the cylinders are assumed to be the same, in accordance with the experiment. Moreover, the radii of the cylinders and the lattice constants are also taken from the experiment. Several values for the acoustic contrasts between the cylinder and the air and different cylinders including the conduit cylinders originally used in the experiment were used in the initial stage of computation. We found that the results are in fact insensitive to the detailed material composition of the cylinders as long as the contrasts exceed a certain value. This agrees with the previous experimental observation [16] and the theoretical results [18]. In the present computation, we also allow the total number of the cylinders to vary from 36 to 500. The cylinders are placed to form a square lattice or a triangular lattice.

Assume that the lattice spacing is $a$, the diameter of the cylinders is $d$. For the square lattice, the filling factor, that is the fraction of the sample area occupied by the scattering cylinders, is calculated as

$$f = \frac{\pi d^2}{4a^2}. \tag{31}$$

For the triangular lattice, the filling factor is given as

$$f = \frac{\pi d^2}{2\sqrt{3}a^2}. \tag{32}$$

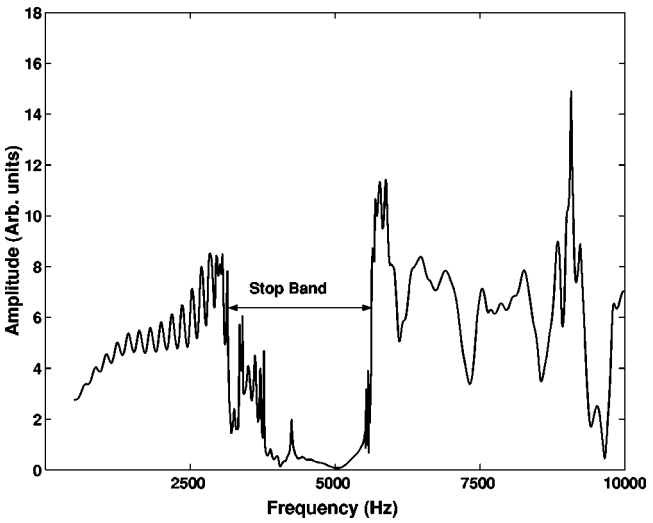


FIG. 1. Transmission as a function of $ka$ along the $\Gamma X$ (i.e., [100]) direction for the square lattice.

Here we note an editorial error in Eq. (2) of [13]. In the experiment carried out in [13], the following parameters are used.

(1) For the square lattice, $a=3.7$ cm and $d=2.34$ cm. This gives a filling factor of 0.31.

(2) For the triangular lattice, for the same cylinders, the filling factor is fixed as 0.366, leading to a spacing of 3.683 cm.

The theoretical results show that the wave transmission is sensitive to the filling factor, as well as the number of the cylinders. In order to limit the possible finite size effects so that they do not obscure the observation of the band gap effects, we found that we need to have more rods than used in the experiment. For frequencies at which wave propagation is possible, there is sensitive interference between the propagating wave and the reflected waves at the boundaries, yielding the familiar pattern of nulls and peaks. If there is a band gap, the transmission will not be possible within the gap. Then the received signal is small, and the transmission will be relatively insensitive to the boundary effects. In other words, the inhibition of a band gap will not be altered by varying the sample size. Our numerical results confirm this.

The transmission spectrum for the square lattice of the rods is presented in Fig. 1 for the propagation along the $\Gamma X$ (i.e., [100]) direction. In the computation, we set the number of cylinders to 200. The transmitter and receiver are placed at such a small distance from the scattering array that the boundary effects do not suppress the band gaps. Here we observe a well defined inhibition regime ranging from about 3 kHz to 5.5 kHz. Within this range of frequency, the transmission is significantly reduced. This agrees very well with the experimental data shown in Fig. 3(a) of [13]. We have also performed a series of numerical tests with respect to changing the number of cylinders or the shape of the array. All results indicate that the regime of inhibition is rather stable. For the transmission outside this regime, however, the transmitted amplitude can vary significantly as the number of scatterers or the shape of the array changes. For example, the transmission through an array of $10\times 20$ will differ from that

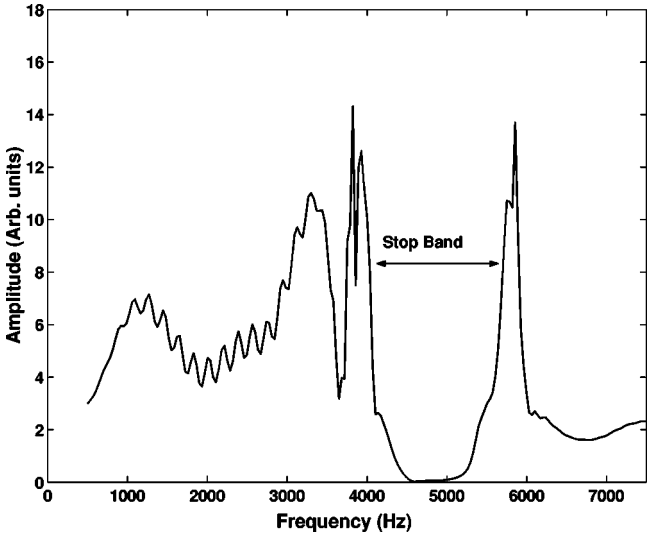


FIG. 2. Transmission as a function of $ka$ along the $\Gamma X$ (i.e., [100]) direction for the triangular lattice.

through an array of $8\times25$, even with the same lattice constant. The oscillatory behavior for frequencies below 2.8 kHz is purely caused by the boundary. They may or may not appear, depending on the arrangement of the array. But the inhibition behavior within the range between 3–5.5 kHz remains quantitatively the same for both arrays. Such a stable inhibition regime is a clear indicator for the stop band. This will be further confirmed by the band structure calculation given below.

We also performed the transmission calculation using Eq. (25) for propagation along the $\Gamma M$ (i.e., [110]) direction. The band structure calculation indicates a small stop band within about 5.6 and 6.0 kHz. Unfortunately, this stop band cannot be clearly identified in our transmission calculation. In the experiment, the transmission data in this case is also less compelling [13]. The authors of [13] then used the phase information extracted from the Fourier transformed data to locate the anomalous phase delay caused by the stop band. Our numerical data on the phase delay is again less convincing. Several reasons may contribute to this. Among others, a prominent reason may be due to the finite number of cylinders. In principle, the stop band from the band structure calculation is obtained for an infinitely large array of scatterers. The fact that there is only a small gap in this situation would imply that a vastly large number of scatterers is required in the transmission calculation. Our present computing facilities, however, do not allow us to simulate the scattering from an array of exceedingly large size.

We also performed numerical computation of the transmission through the triangular lattice. The transmission spectrum is shown in Fig. 2 for wave propagation along the $\Gamma X$ direction. Again we observe a stop band between 4 kHz and 5.7 kHz. This is also in remarkable agreement with the experimental observation, referring to Fig. 4(a) of [13]. The computation of the transmission along the $\Gamma M$ direction is also done. Like in the case of the square lattice, the band structure calculation indicates a narrow stop band within

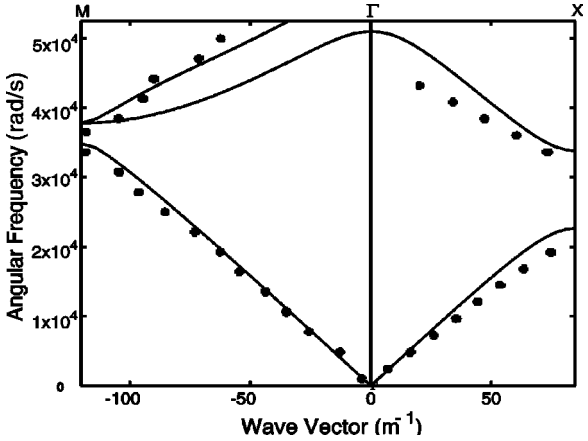


FIG. 3. The theoretical dispersion relation is shown for the square. The experimental data read from [13] are also plotted as the black dots.

about 5.1 and 5.4 kHz. Again the stop band cannot be clearly identified in our transmission calculation.

The theoretical dispersion relation is shown in Figs. 3 and 4 for the square and triangular lattices, respectively. The experimental data read from [13] are also plotted as the black dots in the figures.

First we consider the square lattice case. Overall speaking, the experimental and theoretical data are in a good agreement. The experimental data are only slightly lower than the theoretical prediction. For propagation along the $\Gamma M$ direction, the experimental data agree remarkably well with the theory for the first dispersion curve. For higher frequencies, the experimental data seem to follow third dispersion band, though we see that some experimental data fall on the second band. The agreement between the theory and the experiment is slightly obscured by the presence of three bands near the edge of the Brillouin zone. The theory predicts a small band gap, as discussed earlier. Near the band gap, the theory and the experiment are in a slight discrepancy. Again, for the transmission along the $\Gamma X$ direction, the

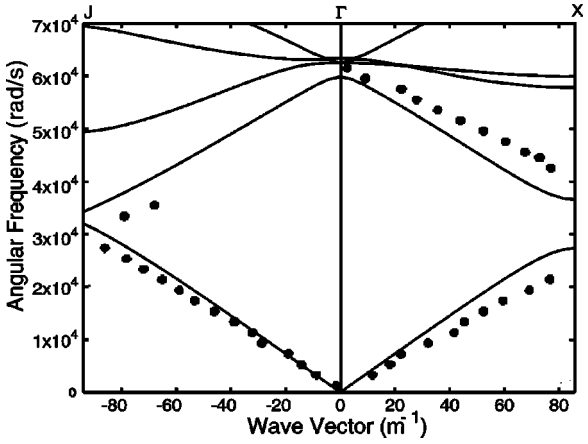


FIG. 4. The theoretical dispersion relation is shown for the triangular lattices. The experimental data read from [13] are also plotted as black dots.

agreement in the lower dispersion band appears better than in the higher band. A reason may be that the phase is relatively hard to accurately measure at high frequencies. For both bands, the experimental data are lower than the predicted values. Comparing the band structure results in Fig. 3 with the transmission results in Fig. 1, we see that the stop band predicted from the transmission spectrum is also slightly shifted toward lower frequencies. The further computation indicates that such a very small shift is due to the finite number of cylinders. Increasing the number of scatterers will lift a bit the stop band in the transmission spectrum.

Now we consider the triangular lattice. Again, from Fig. 4 we see that the agreement between the theory and the experiment is genuinely good, considering the complication involved in the experiment. However, there are a few small discrepancies. First, the experiment observes a wider stop band along the $\Gamma X$ direction, and the experimental observation of the stop band along the $\Gamma M$ direction is not so obvious. From Fig. 4, we see that the two lowest dispersion bands are observed by experiment. In the triangular lattice case, the stop band estimated from the transmission spectrum from Fig. 2 agrees with the dispersion band calculation in the $\Gamma X$ direction.

## IV. SUMMARY

In conclusion, in this paper we have presented a theoretical analysis of the acoustic propagation through two-dimensional regular arrays of parallel cylinders in air. A self-consistent method is used to compute the wave transmission, taking into account all orders of multiple scattering. We stress that this approach in fact allows us to consider any configuration of the scattering arrays. For the regular arrays, the plane-wave method is used to calculate the band structures. Two lattice arrangements are considered. The theory are then applied to the experimental situations, yielding favorable agreements.

## ACKNOWLEDGMENT

The work received support from National Science Council of ROC.

[1] A. Ishimaru, *Wave Propagation and Scattering in Random Media* (Oxford University Press, New York, 1997).
[2] Z. Ye, J. Appl. Phys. **78**, 6389 (1995).
[3] Z. Ye, T. Curran, and D. Lemon, ICES J. Mar. Sci. **53**, 317 (1996).
[4] S. Datta, *Electronic Transport in Mesoscopic Systems* (Cambridge University Press, New York, 1995).
[5] C. Kittel, *Introduction to Solid State Physics* (Wiley, New York, 1996).
[6] E. Yablonovitch, Phys. Rev. Lett. **58**, 2059 (1987); S. John, *ibid.* **58**, 2486 (1987).
[7] Please refer to http://www.home.earthlink.net/~jpdowling/pbgbib.html.
[8] W. Robertson *et al.*, Phys. Rev. Lett. **68**, 2023 (1992).
[9] J. D. Joannopoulos, R. D. Meade, and J. N. Winn, *Photonic Crystal-Molding the Flow of Light* (Princeton University Press, Princeton, NJ, 1995).
[10] A. Diez, G. Kakarantzao, T. Birks, and P. St. J. Russell, Appl. Phys. Lett. **76**, 3481 (2000).
[11] M. Ibanescu, Y. Fink, S. Fan, E. L. Thomas, and J. D. Joannopoulos, Science **289**, 415 (2000).
[12] A. R. Parker, R. C. McPhedran, D. R. McKenzie, L. C. Botton, and N. P. Nicorovici, Nature (London) **409**, 36 (2001).
[13] W. M. Robertson and J. F. Rudy III, J. Acoust. Soc. Am. **104**, 694 (1998).
[14] M. S. Kushwaha, Int. J. Mod. Phys. B **10**, 977 (1996).
[15] R. Martínes-Sala *et al.*, Nature (London) **378**, 241 (1995).
[16] J. V. Sánchez-Pérez *et al.*, Phys. Rev. Lett. **80**, 5325 (1998).
[17] M. S. Kushwaha, Appl. Phys. Lett. **70**, 3218 (1997).
[18] Y. Y. Chen and Z. Ye, e-print cond-mat/0101442, http://xxx.lanl.gov/abs/cond-mat/0101442.
[19] V. Twersky, J. Acoust. Soc. Am. **24**, 42 (1951).
[20] I. S Gradshteyn, I. M. Ryzhik, and A. Jeffrey, *Table of Integrals, Series, and Products*, 5th ed. (Academic Press, New York, 1994).